Supporting Information for

Coupled diffusion in lipid bilayers upon close approach

Sander Pronk, Erik Lindahl, and Peter M. Kasson

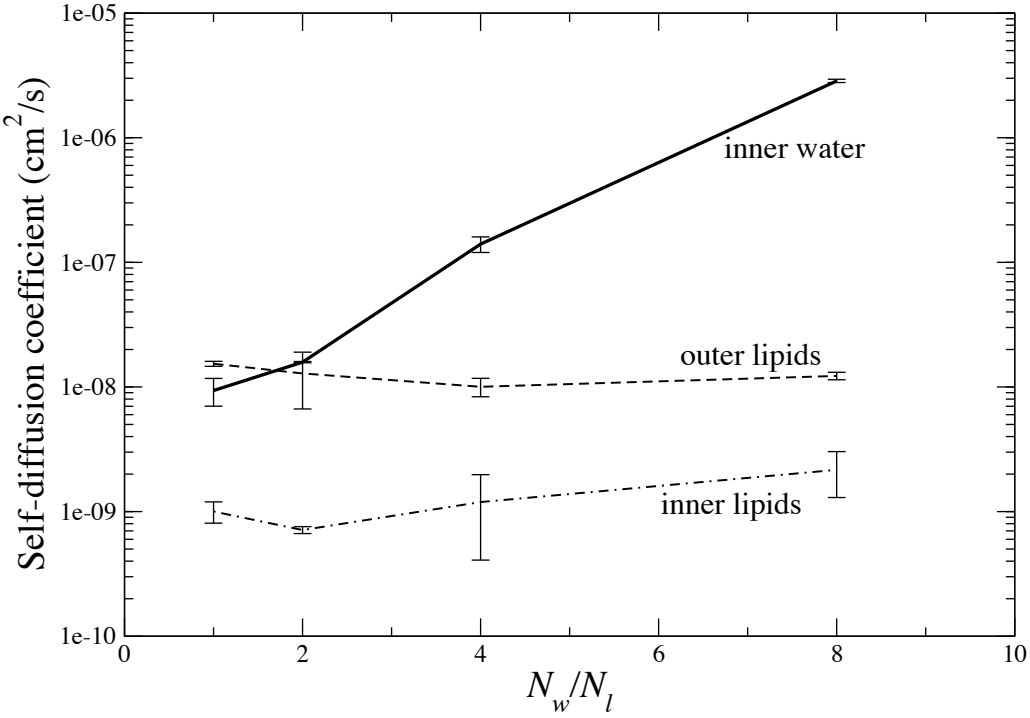

Figure S1. Slowed lateral diffusion at interfaces between bilayers of asymmetric density. Estimated self-diffusion coefficients are plotted for outer-leaflet lipids, inner-leaflet lipids, and interfacial water. These coefficients show a pattern of slowed inner-leaflet and interfacial water diffusion similar to that observed in bilayers of symmetric lipid density (Figure 3).

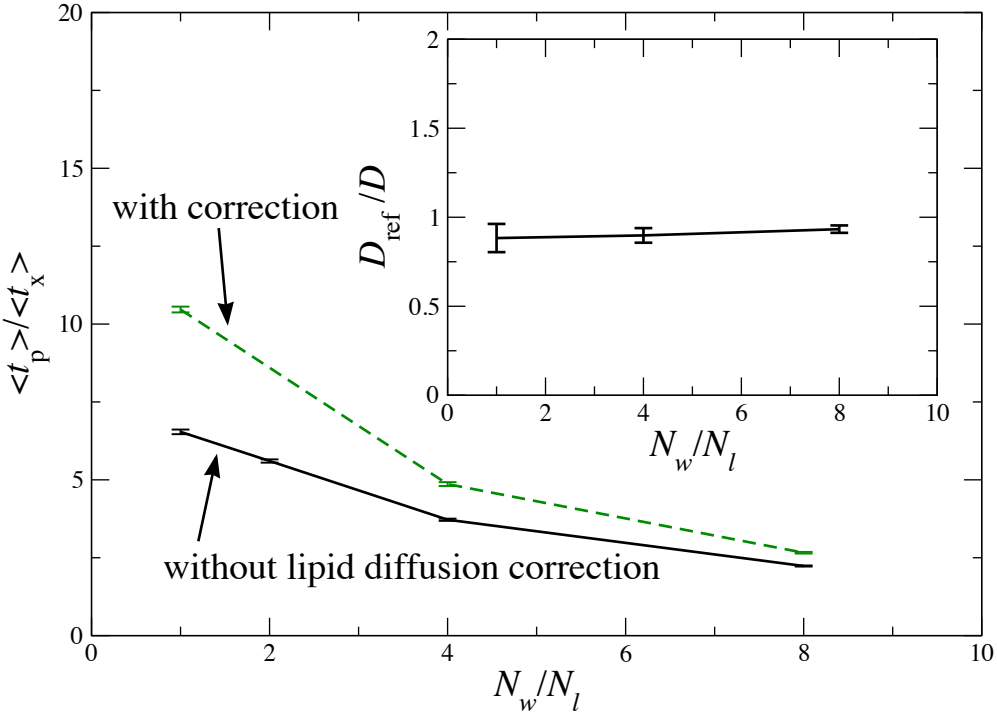

Figure S2. Diffusion-viscosity decoupling and coupled diffusion between bilayers of asymmetric density. The ratio of average persistence and exchange times is plotted for water molecules located between the two bilayers. Dynamic heterogeneity is readily apparent to a roughly similar degree as for bilayers of symmetric density (Figure 7). The inset shows diffusional coupling between inner bilayer leaflets. The ratio of coupled (D_{ref}) to uncoupled (D) diffusion coefficients is plotted in a similar fashion to Figure 4. In the range of 1-8 water molecules per inner leaflet lipid, this ratio was slightly below 1, whereas the ratio would approach 2 in the case of uncorrelated diffusion in the two inner leaflets.

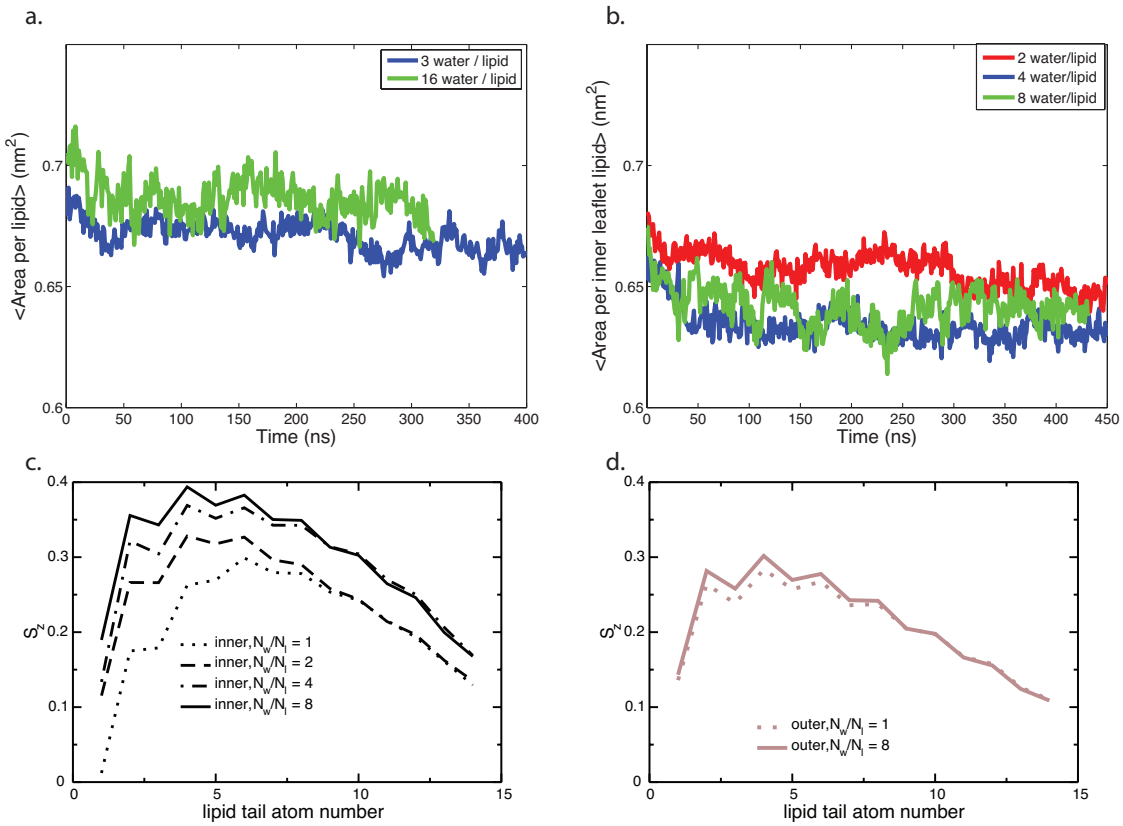

Figure S3. Effect of lipid density on bilayer structural parameters. Plotted in panels (a) and (b) are average area per inner-leaflet lipid in bilayers of symmetric lipid density (a) and bilayers where the inner-leaflet lipid lateral density was 10% higher than the outer-leaflet lipid lateral density (b). A vertical dashed line denotes the start of production simulations in the bilayers of asymmetric density. Plotted in panels (c) and (d) are acyl tail order parameters for bilayers of asymmetric lipid density in the inner and outer leaflets, respectively. Order parameters values are higher for the inner leaflets than the outer, as would be expected for higher lateral density in the inner leaflets.

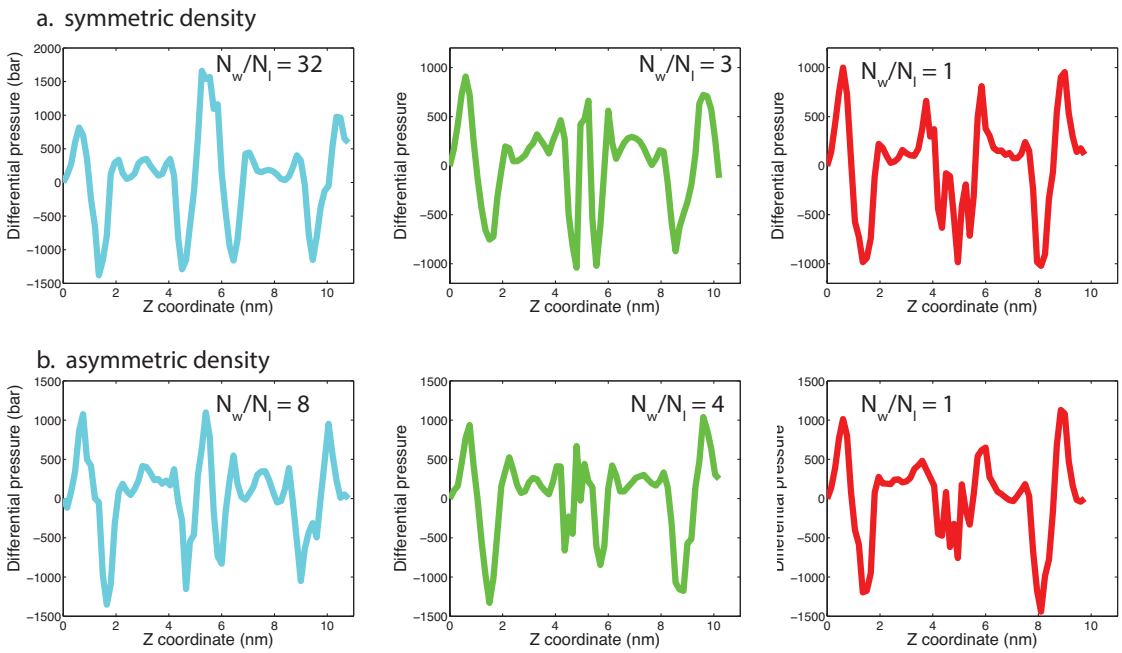

Figure S4. Effect of lipid density on lateral tension in the bilayer. Differential pressure profiles are plotted in bar for bilayers of symmetric (a) and asymmetric (b) lipid lateral density at varying levels of hydration. Differential pressure yields surface tension if integrated across the system. Local pressure calculations were performed using a pressure grid spacing of 0.15 nm on simulation frames spaced every 4 ns.

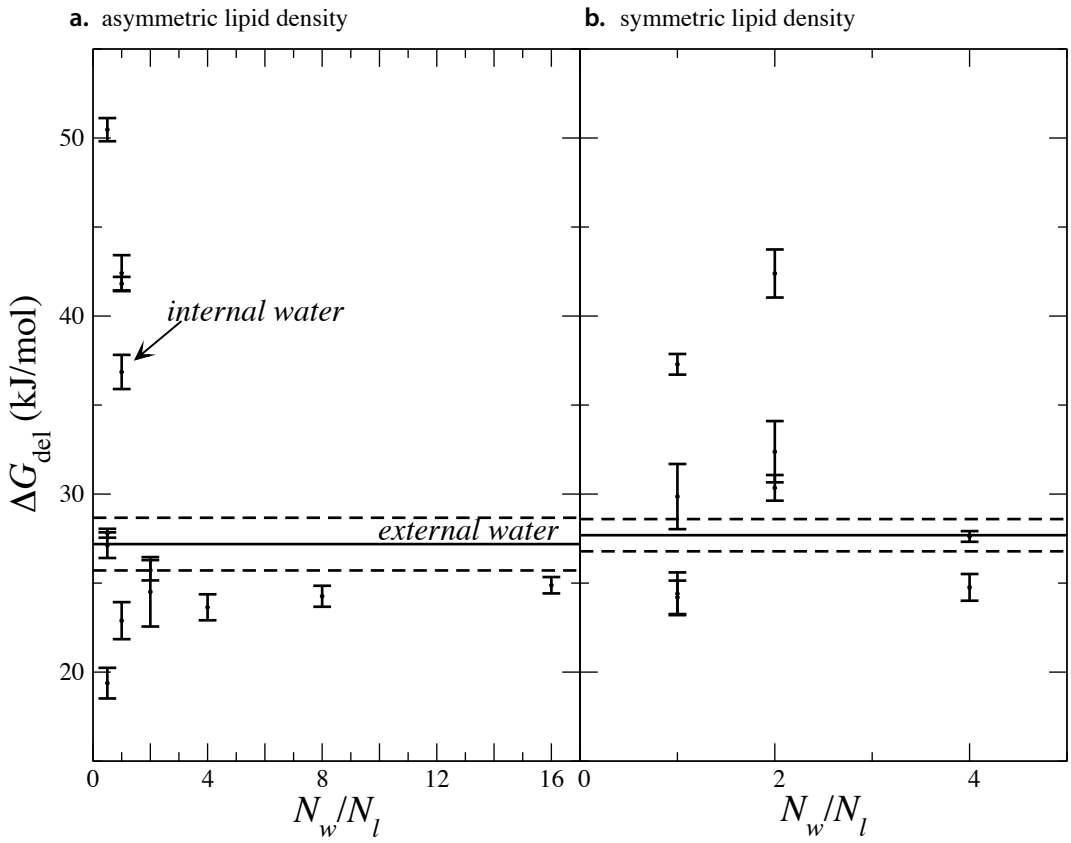

Figure S5. Chemical potential of water probed via free energies of removal. Panels (a) and (b) show the free energy of removing one molecule of water from the "internal" region between bilayers relative to the "external" well-hydrated region (plotted as a solid line with dashed lines at +/- 1 standard error). The free energy of water transfer from external to internal regions can thus be determined as the difference between the free energies of water removal. Free energies were calculated by randomly selecting a water molecule from the designated region and performing free energy perturbation as described in the Methods. Note that the free energy ΔG does not account for components common to both the internal and external molecules such as the removal of constraints in vacuum. At low water-to-lipid ratios (N_w / N_l < 2), the free energy as measured by simulations becomes strongly dependent on the interaction state of the bilayer with the specific water molecule being deleted. This can be seen in highly divergent free energy values for different randomly selected water molecules. At higher water-to-lipid ratios, the chemical potentials of the inner and outer region approach equality.